International Journal of Coal Science & Technology (2022) 9:57
https://doi.org/10.1007/s40789-022-00527-8

RESEARCH

Thermodynamics fundamentals and energy efficiency for the separation and high-valued utilization of Fischer–Tropsch heavy oil

Zongchao Liu[1] · Hong Li[1] · Suli Liu[2] · Jiuzhou Chen[2] · Zisheng Zhang[1,4] · Xingang Li[1] · Angui Zhang[2] · Wei Yuan[2] · Xin Gao[1,3]

Received: 12 February 2022 / Accepted: 16 June 2022

Abstract
The development trend of Fischer–Tropsch (F–T) technology is to develop high value-added products. The separation of linear α-olefins with low cost is an effective method. Nevertheless, the lack of thermodynamic data and the huge energy consumption are the two main problems restricting the development of the separation process. The thermodynamic data of the key components (1-dodecene and *n*-dodecane) in the F–T product were measured. The Wilson binary interaction parameters of the key components were obtained. Next, one traditional distillation column sequence and two dividing wall column (DWC) sequences were designed to separate the F–T heavy oil to obtain narrow fractions with different carbon numbers. Then, the obtained fractions of C10 and C12 were simulated to obtain 1-decene and 1-dodecene, respectively. There was a traditional distillation and a differential pressure thermal coupling distillation process. When separating 95.0% purity 1-decene and 1-octene, the direct DWC process and differential pressure thermal coupled distillation are an excellent combination, which can reduce the energy by 33.1% (i.e., 11,286 kW) and total annual cost by 15.9% (i.e., 3.96×10^6 \$) compared with traditional distillation.

Keywords F–T synthesis · α-Olefins · DWC · Heat-integrated distillation · Process design

1 Introduction

The Fischer–Tropsch (F–T) synthesis process (Fischer and Tropsch 1923; Leckel 2009) is a process of directly or indirectly converting solid energy into liquid fuels or chemicals. The process is mainly the coal-to-oil process. However, if liquid fuels are the main product, there is no competitive when oil prices are low (Choi 1997; Dry and Steynberg 2004). The F–T products are usually a variety of alkanes and alkenes, especially the normal alkenes, with a little oxygenated compound. The majority of alkenes are α-olefins which have a high economic value. Furthermore, sulfur, nitrogen, and aromatic hydrocarbons are very low (Egaña et al. 2018; Muleja et al. 2017; Nakhaei Pour et al. 2018). 1-decene and 1-dodecene in linear α-olefins are the vital chemical raw materials for the production of surfactants, lubricants, and other products (Greiner et al. 2004). And the demand for 1-decene and 1-dodecene has been increasing nowadays. In addition, oligomerization of ethylene and F–T synthesis are the main methods to produce linear α-olefins. Ethylene oligomerization (Belov and Matkovsky 2010; Dixon et al. 2004) requires high cost and great environmental pollution. Moreover, the products conform to Poisson distribution. The F–T synthesis method is a process developed and used exclusively by the Sasol company in South Africa. The process separate high-quality linear α-olefins from the F–T flow through pre-separation, super-distillation, extractive distillation, and other steps (De Klerk 2012). However,

Zongchao Liu and Hong Li have contributed equally.

✉ Xin Gao
gaoxin@tju.edu.cn

1 School of Chemical Engineering and Technology, National Engineering Research Center of Distillation Technology, Tianjin University, Tianjin 300072, China

2 Ningxia Coal Industry Group Co. Ltd., CHN ENERGY, Yinchuan 750011, China

3 Haihe Laboratory of Sustainable Chemical Transformations, Tianjin 300192, China

4 Department of Chemical and Biological Engineering, University of Ottawa, Ottawa K1N 6N5, Canada

Published online: 08 August 2022

Sasol company can only separate 1-pentene, 1-hexene, and 1-octene from F–T oil. There is no mature technology to separate 1-decene and 1-octene from F–T oil. At present, the methods for separating long-chain linear α-olefins from F–T synthetic oil include adsorption, complexation, and extraction (Ge 2014; Mi 2017; Wang 2016). Compared with distillation, efficient and safe third-party reagents required for adsorption, complexation and extraction are difficult to determine. The other separation methods require less energy consumption than distillation if suitable reagents are available.

The initial separation of F–T synthetic oil is a typical multi-component distillation process. The energy consumption accounts for most of the capital cost. Therefore, the energy-saving design of F–T synthesis oil separation has become an important driving force for the development of F–T synthesis plants. In this respect, the DWC technology is a better choice. One DWC which realizes the thermal coupling between the two columns can produce two products at the same time (da Cunha et al. 2018; Kaibel 1987; Petlyuk 1965). Thus, it can reduce equipment investment costs. Meanwhile, the DWC reduces back mixing. It provides substantial energy savings of approximately 30% compared to traditional distillation (Schultz et al. 2002). Therefore, the application of DWC technology has a significant energy-saving effect for the separation of F–T synthetic oil. However, The F–T oil containing hundreds of compounds is difficult to converge in the simulation. Therefore, a single-tower model with better convergence is used when simulating (Dejanović et al. 2010), which is the MultiFrac module in Aspen V11. Moreover, the economics of different DWC separation sequence is also different. It is mainly reflected in the operating cost (Yildirim et al. 2011).

Also, the products obtained from the initial separation of F–T oil are only mixtures, which contains α-olefins and other components with similar boiling point. To obtain α-olefins, especially 1-decene and 1-dodecene, differential pressure thermally coupled distillation (DPTD) can be adopted as a very effective method (Li et al. 2008; Zhang et al. 2015). In the DPTD process, a traditional distillation tower is replaced by two towers. The materials are transferred through a throttle valve and a compressor. The condenser of the rectifying section operating at high pressure is more than 10 °C higher than the reboiler of the stripping section operating at low pressure. Therefore, the condenser can transfer heat to the reboiler so that only a small amount of external energy is required. However, the heat of the reboiler and the condenser cannot be completely coupled, so an additional reboiler or condenser is required. In addition, the cost of compressor and electricity needs to be considered, but it is small compared to the cost savings.

In this study, we measured the thermodynamic data of a set of key components (i.e., 1-dodecene and *n*-dodecane) and adopted a set of existing thermodynamic data (i.e., 1-decene and *n*-decane) (Wang et al. 2016). The thermodynamic data was used to improve the accuracy of the simulation. The thermodynamic consistency adopts the Van Ness test. Then, one traditional distillation separation sequence (TDS) process and two DWC processes, including an indirect DWC process (IDWC) and a direct DWC process (DDWC), were simulated and optimized to obtain fractions from F–T oil. Meanwhile, one traditional distillation (TD) process and one DPTD process were simulated and optimized to acquire α-olefins (i.e., 1-decene and 1-dodecene) from C10 and C12 fractions. The reboiler duty and TAC of different separation sequences in the same procedure have been optimized and compared.

2 Thermodynamic data acquisition

2.1 Phase equilibrium experiment

The information on the reagents (i.e., 1-dodecene and *n*-dodecane) used are listed in Table S1 of supplementary material.

Our research uses a vapor–liquid double circulation balance kettle, which has been used by our team (Gao et al. 2019; Li et al. 2014, 2016, 2018). The vapor–liquid balance device is shown in Fig. 1. The vapor–liquid equilibrium process takes place in the equilibrium chamber. Both vapor and liquid circulate in the device, reducing balance time and improving measurement accuracy. The apparatus was operated under vacuum conditions, and the measurement accuracy of the vacuum gauge (HC-YS100, Ru Yi Instruments, Shanghai) was ± 0.4 kPa. Meanwhile, we calibrated the vacuum gauge with ultrapure water. The temperature was measured by a thermocouple thermometer (1552A-Ex,

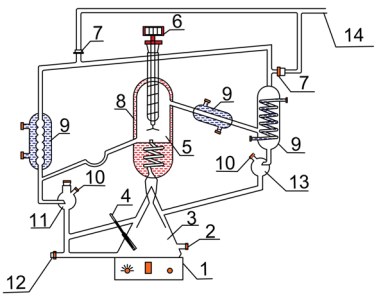

Fig. 1 The vapor–liquid double circulation balance kettle: 1-magnetic heating stirrer; 2-feeding port; 3-evaporation chamber; 4-thermometer; 5-equilibrium room; 6-thermocouple thermometer; 7-junction port; 8-insulation layer; 9-condenser chamber; 10-sampling port; 11-liquid-phase returning section; 12-discharge port; 13- vapor-phase returning section and 14-vacuum port

Fluke, USA) which the accuracy was ± 0.01 K. The experiment's procedure is in supporting information.

Gas chromatography (Clarus 690, PE, USA) was used to analyze the compositions of vapor and liquid samples with PONA chromatographic column (50 m × 0.2 mm × 0.5 μm, Agilent) and flame ionization detector (FID). The nitrogen (mass fraction 0.99999) carrier gas flow rate was 1.0 mL/min. The flow rates of hydrogen and air were 35 and 350 mL/min, respectively. The sample injection volume was 0.5 μL, and the split ratio was 150:1. The temperature of the injector was 533.15 K as well as the detector. The chromatographic column temperature was 413.15 K for 20 min. Each sample was analyzed at least three times to ensure that the error is within ± 0.5%, and use the averaged data. The method used to analyze the measured chromatographic data was area normalization method.

2.2 Experimental results and consistency test

The results of VLE data for 1-dodecene and *n*-dodecane are shown in Tables S2 in Supplmentary Material. Assuming that the liquid and gas phases are both non-ideal, the activity coefficient γ_i was calculated by Eq. (1).

$$\varphi_i y_i p = x_i \gamma_i \varphi_i^V p_i^s \exp\left(\frac{1}{RT}\int_c^p V_i^1 \mathrm{d}p\right) \tag{1}$$

where x_i represents the liquid phase molar fractions of component i as well as y_i represents the vapor phase molar fractions, T represents the temperature, φ_i and φ_i^V represent the fugacity coefficients of component i in the mixture system and pure system, respectively, p represents the total pressure, p_i^s represents the saturated vapor pressure of component i, γ_i represents the activity coefficient of component i in the liquid phase, and V_i^1 represents the liquid molar volume of component i.

The p_i^s could be obtained from the (Eq. 2).

$$\ln p_i^s = C_{1i} + \frac{C_{2i}}{T + C_{3i}} + C_{4i}T + C_{5i}\ln T + C_{6i}T^{C_{7i}}, C_{8i} \le T \le C_{9i} \tag{2}$$

where $C_{(1-7)i}$is the Antoine parameter as well as C_{8i} and C_{9i} are the effective range of the temperature. $C_{(1-9)i}$ were shown in Table S3 in Supplmentary Material.

The measured gas–liquid equilibrium data needs to be checked for thermodynamic consistency which principle is the Gibbs–Duhem equation (Valderrama et al. 2019). Thermodynamic consistency inspection can be divided into integral inspection (i.e., area test) (Fredenslund 2012; Herington 1951) and point-by-point inspection (i.e., point test). The activity coefficients of 1-dodecene and *n*-dodecane are close to 1.0 as shown in Table S2 in Supplementary Material, which are highly ideal systems so that the area test is not applicable (Kang et al. 2010; Yamamoto and Narahara 2004). The second verification method Van Ness and his colleagues researched in this regard.

The Van Ness test (Liu et al. 2018) (i.e., point test) is used to verify each data point, the parameters involved are calculated by Eqs. (3) and (4):

$$\Delta p = \frac{1}{N}\sum_{i=1}^{N}\Delta p_i = \frac{1}{N}\sum_{i=1}^{N} 100\left|\frac{p_i^{\exp} - p_i^{\mathrm{cal}}}{p_i^{\exp}}\right| \tag{3}$$

$$\Delta y = \frac{1}{N}\sum_{i=1}^{N}\Delta y_i = \frac{1}{N}\sum_{i=1}^{N} 100\left|y_i^{\exp} - y_i^{\mathrm{cal}}\right| \tag{4}$$

where N represents the number of experimental points, exp and cal represent the parameters as experimental and simulated values, respectively, where the simulated values are calculated by different thermodynamic models. As shown in Table S4 of Supplementary Material, Δp and Δy that calculated by three activity coefficient models (Wilson, NRTL, and UNIQUAC) are both less than 1, indicating that the experimental data passes the thermodynamic consistency test and the experimental data is valid.

2.3 Data regression

Three different activity coefficient models (Wilson, NRTL, and UNIQUAC) were used to regress from the experimental data of 1-dodecene and *n*-dodecane to check the thermodynamic consistency and obtain the binary interaction parameters of the three models. The correlation equation is Eq. (5)

$$OF = \sum_{i=1}^{N}\left[\left(\frac{T_i^{\exp} - T_i^{\mathrm{cal}}}{\sigma^T}\right)^2 + \left(\frac{p_i^{\exp} - p_i^{\mathrm{cal}}}{\sigma^p}\right)^2 + \left(\frac{x_i^{\exp} - x_i^{\mathrm{cal}}}{\sigma^x}\right)^2 + \left(\frac{y_i^{\exp} - y_i^{\mathrm{cal}}}{\sigma^y}\right)^2\right] \tag{5}$$

where σ is the standard deviation.

Table S2 summarizes the absolute difference of temperature (i.e., ΔT) and vapor-phase molar fraction of 1-dodecene (i.e., Δy_i) between the calculated values of the three thermodynamic models and the experimental values. The vapor pressure model parameters were adjusted to matching the experimental and fitted values for the pure components, as shown in Table S3 in Supplementary Material.

The root-mean-square deviation (RMSD) is used to express the degree of correlation between the experimental value and the calculated value. Table S4 summarizes the RMSD of the temperature (RMSD (T)) and the gas-phase molar fraction of 1-dodecene (RMSD (y_i)) for the three models. RMSD (T) and RMSD (y_i) are calculated by Eqs. (6) and (7).

$$\mathrm{RMSD}\,(T) = \sqrt{\frac{1}{N}\sum\left(T^{\mathrm{cal}} - T^{\exp}\right)^2} \tag{6}$$

$$\mathrm{RMSD}\left(y_i\right)=\sqrt{\frac{1}{N}\sum\left(y_i^{\mathrm{cal}}-y_i^{\mathrm{exp}}\right)^2} \tag{7}$$

Figure 2 shows the gas–liquid equilibrium data of 1-dodecene and *n*-dodecane and the regression values of the three thermodynamic models (Wilson, NRTL, and UNIQUAC) on the experimental data. The absolute difference and RMSD showed from Table S4 are particularly low indicating that the obtained thermodynamic data is valid. However, there are some differences between the experimental results and the theoretical correlated results. This may be due to systematic errors in experiment and ideality of the model. Wilson has the better correlation with the experimental value, so the Wilson model is used to separate 1-dodecene from the C12 fractions in the simulation. Wilson's binary interaction parameters are shown in Table S5 in Supplementary Material.

3 Process design and simulation

In this part, the F–T heavy oil separation processes as well as normal olefins and alkanes' (i.e., C10 and C12) separation processes were simulated. Then the processes were optimized with the goal of column heat load using Aspen Plus V11. Three processes for separating F–T heavy oil were designed, including a TDS process, an IDWC process, and a DDWC process. Moreover, the TD process was modeled to acquire 1-decene and 1-dodecene and optimized for column heat load. Then we established the DPTD process based on TD process. The thermodynamic model of F–T heavy oil separation was the BK-10 which was suitable for wide boiling point range under reduced pressure while normal olefins and alkanes' separation were the Wilson. The BK-10 was developed from the charts for both real components and oil fractions. The parameters for BK-10 are all built-in so that not need to supply them. To improve the accuracy of the second process simulation, this study searched some thermodynamic data in literature. Import the thermodynamic data acquired into Aspen Plus V11 for the simulation of α-olefin separation from narrow cut. The Wilson interaction parameters involved in the simulation are shown in Table S5. The logic optimization of DWC is shown in Fig. 3 with the optimization logic targeting reboiler duty is shown in Fig. 3a.

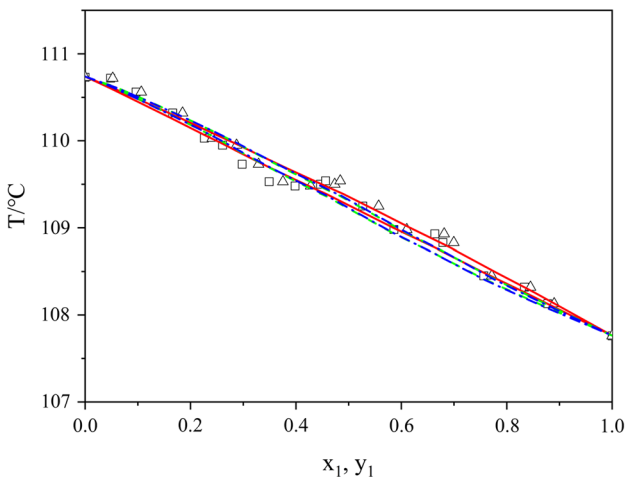

Fig. 2 Gas–liquid equilibrium diagram for the 1-dodecene (1) + *n*-dodecane (2) at 3.36 kPa. Square, triangle, (x_1, y_1) measurement data; red line, (x_1, y_1) Wilson model fitting results; green dashed line, (x_1, y_1) NRTL model fitting results; blue dashed line, (x_1, y_1) UNIQUAC model fitting results.

3.1 F–T heavy oil separation process simulation

The products of F–T heavy oil's initial separation were C8–C9, C10, C11, C12, C13, C14–C18, C19+ narrow fractions. Among them, the C19+ fractions refer to the narrow fraction of C19 and the components with a boiling point greater than *n*-nonadecane. The composition of the F–T heavy oil is summarized in Table S6. The feed rate is 73,009 kg/h, corresponding to the four million tons coal-to-liquid scale, with 150 °C and 101.32 kPa. The operating pressure of the tower is 3.5 kPa so that the temperature of the tower kettle will not be too high to cause coking of the material. The product's design specification is 96 wt%. The product refers to a narrow fraction containing α-olefins with different carbon numbers and components with similar boiling point to the corresponding α-olefins. The three separation processes of F–T heavy oil are shown in Fig. 4. The parameters were obtained with TAC as the optimization goal.

For the TDS process (Fig. 4a), a design specification was made that the reflux ratio changes to ensure the purity of the top product. The pressure drop on the tray makes the number of trays have an optimal value. These distillation towers were optimized for the number of trays, top distillation rate, and feed position to minimize the reboiler duty.

The DWC which has a total of ten degrees of freedom is more difficult to design than the traditional distillation column with four degrees of freedom. Taking into account the diversity of F–T oil components, a single-tower model is used to design to make the calculation easier to converge. In the design, two-thirds of the number of plates in the two traditional distillation towers is usually used as the number of main tower plates in the DWC. This value is usually unchanged or changes very little during optimization, so we finally optimize the number of main tower plates. The number of plates in the initial distillation tower is usually one-third of the number of the main tower plates, and the placement of the dividing wall is at one-third of the main tower. Some design specifications were made that the reflux ratio and gas distribution ratio to ensure the quality of the

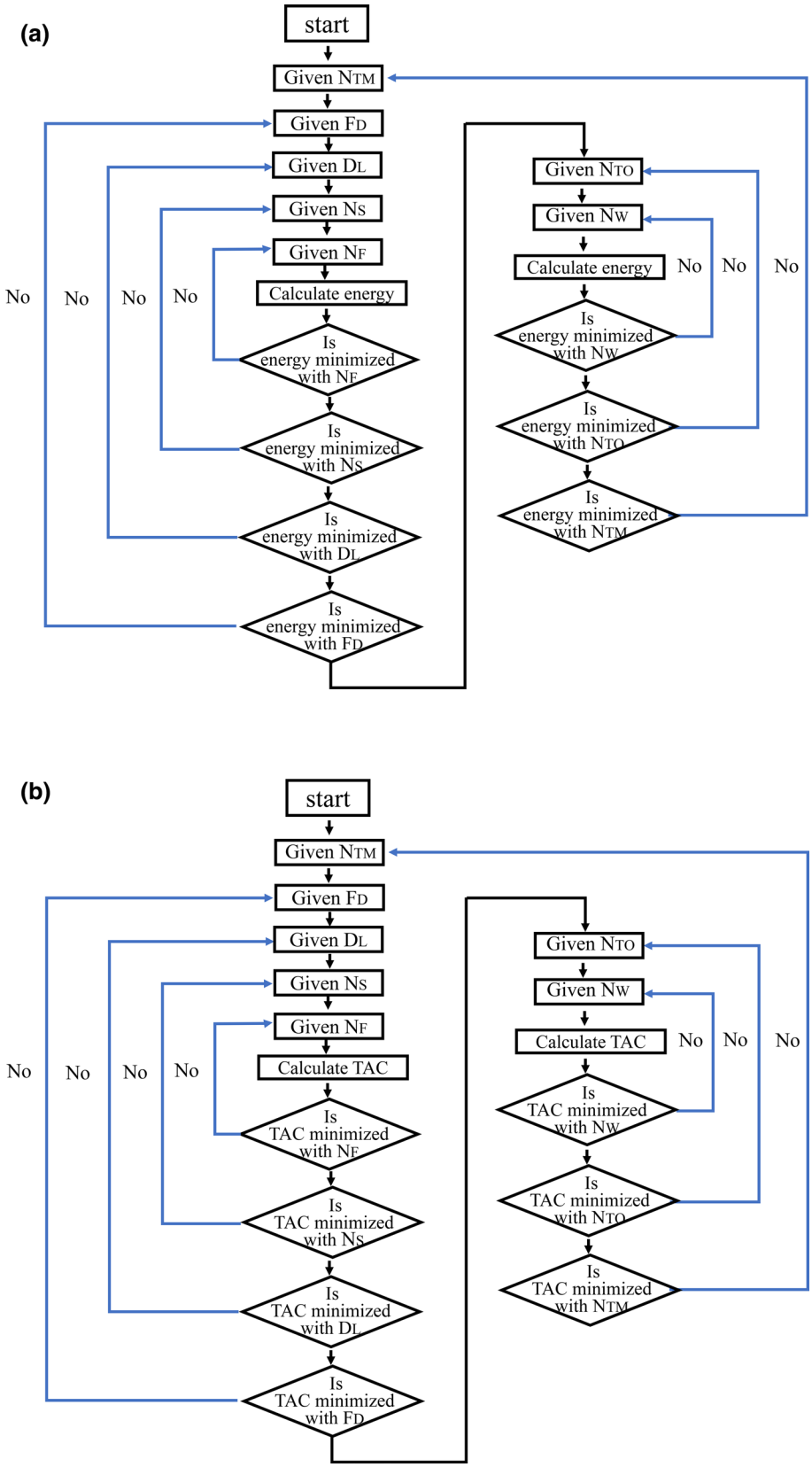

Fig. 3 DWC optimization logic. **a** Energy minimum optimization logic; **b** TAC minimum optimization logic

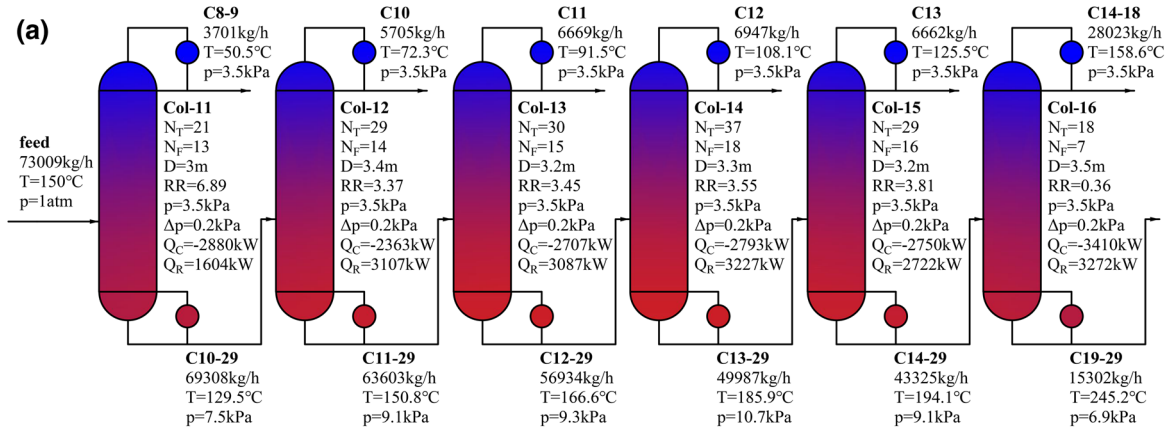
(a)
feed
73009kg/h
T=150°C
p=1atm
Col-11
NT=21
NF=13
D=3m
RR=6.89
p=3.5kPa
Δp=0.2kPa
QC=-2880kW
QR=1604kW
C8-9
3701kg/h
T=50.5°C
p=3.5kPa
C10-29
69308kg/h
T=129.5°C
p=7.5kPa
Col-12
NT=29
NF=14
D=3.4m
RR=3.37
p=3.5kPa
Δp=0.2kPa
QC=-2363kW
QR=3107kW
C10
5705kg/h
T=72.3°C
p=3.5kPa
C11-29
63603kg/h
T=150.8°C
p=9.1kPa
Col-13
NT=30
NF=15
D=3.2m
RR=3.45
p=3.5kPa
Δp=0.2kPa
QC=-2707kW
QR=3087kW
C11
6669kg/h
T=91.5°C
p=3.5kPa
C12-29
56934kg/h
T=166.6°C
p=9.3kPa
Col-14
NT=37
NF=18
D=3.3m
RR=3.55
p=3.5kPa
Δp=0.2kPa
QC=-2793kW
QR=3227kW
C12
6947kg/h
T=108.1°C
p=3.5kPa
C13-29
49987kg/h
T=185.9°C
p=10.7kPa
Col-15
NT=29
NF=16
D=3.2m
RR=3.81
p=3.5kPa
Δp=0.2kPa
QC=-2750kW
QR=2722kW
C13
6662kg/h
T=125.5°C
p=3.5kPa
C14-29
43325kg/h
T=194.1°C
p=9.1kPa
Col-16
NT=18
NF=7
D=3.5m
RR=0.36
p=3.5kPa
Δp=0.2kPa
QC=-3410kW
QR=3272kW
C14-18
28023kg/h
T=158.6°C
p=3.5kPa
C19-29
15302kg/h
T=245.2°C
p=6.9kPa

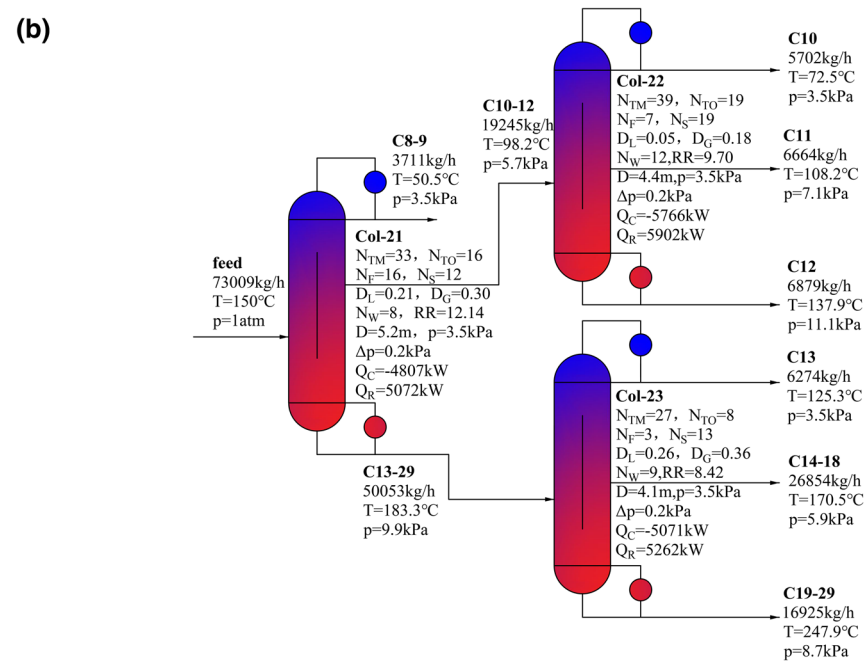
(b)
feed
73009kg/h
T=150°C
p=1atm
Col-21
NTM=33, NTO=16
NF=16, NS=12
DL=0.21, DG=0.30
NW=8, RR=12.14
D=5.2m, p=3.5kPa
Δp=0.2kPa
QC=-4807kW
QR=5072kW
C8-9
3711kg/h
T=50.5°C
p=3.5kPa
C10-12
19245kg/h
T=98.2°C
p=5.7kPa
C13-29
50053kg/h
T=183.3°C
p=9.9kPa
Col-22
NTM=39, NTO=19
NF=7, NS=19
DL=0.05, DG=0.18
NW=12,RR=9.70
D=4.4m,p=3.5kPa
Δp=0.2kPa
QC=-5766kW
QR=5902kW
C10
5702kg/h
T=72.5°C
p=3.5kPa
C11
6664kg/h
T=108.2°C
p=7.1kPa
C12
6879kg/h
T=137.9°C
p=11.1kPa
Col-23
NTM=27, NTO=8
NF=3, NS=13
DL=0.26, DG=0.36
NW=9,RR=8.42
D=4.1m,p=3.5kPa
Δp=0.2kPa
QC=-5071kW
QR=5262kW
C13
6274kg/h
T=125.3°C
p=3.5kPa
C14-18
26854kg/h
T=170.5°C
p=5.9kPa
C19-29
16925kg/h
T=247.9°C
p=8.7kPa

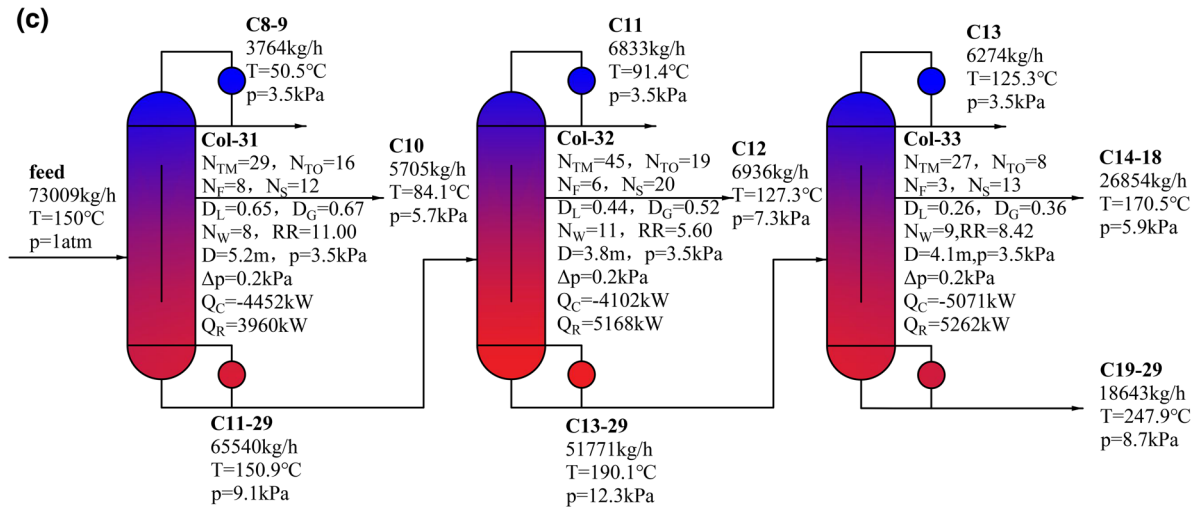
(c)
feed
73009kg/h
T=150°C
p=1atm
Col-31
NTM=29, NTO=16
NF=8, NS=12
DL=0.65, DG=0.67
NW=8, RR=11.00
D=5.2m, p=3.5kPa
Δp=0.2kPa
QC=-4452kW
QR=3960kW
C8-9
3764kg/h
T=50.5°C
p=3.5kPa
C11-29
65540kg/h
T=150.9°C
p=9.1kPa
Col-32
NTM=45, NTO=19
NF=6, NS=20
DL=0.44, DG=0.52
NW=11, RR=5.60
D=3.8m, p=3.5kPa
Δp=0.2kPa
QC=-4102kW
QR=5168kW
C10
5705kg/h
T=84.1°C
p=5.7kPa
C11
6833kg/h
T=91.4°C
p=3.5kPa
C13-29
51771kg/h
T=190.1°C
p=12.3kPa
Col-33
NTM=27, NTO=8
NF=3, NS=13
DL=0.26, DG=0.36
NW=9,RR=8.42
D=4.1m,p=3.5kPa
Δp=0.2kPa
QC=-5071kW
QR=5262kW
C12
6936kg/h
T=127.3°C
p=7.3kPa
C13
6274kg/h
T=125.3°C
p=3.5kPa
C14-18
26854kg/h
T=170.5°C
p=5.9kPa
C19-29
18643kg/h
T=247.9°C
p=8.7kPa

◂**Fig. 4** Process and simulation results of F–T heavy oil. **a** Traditional direct distillation sequence process; **b** Indirect dividing wall column process; **c** Direct dividing wall column process

products extracted from the top and sidelines of the tower. Optimizing the product quality of the tower kettle with the flow rate of sideline production. These DWCs were optimized for the number of main tower plates, the number of initial distillation tower plates, dividing wall position, top distillation rate, liquid distribution ratio, sideline position, and feed position to minimize energy consumption.

For the IDWC separation sequence (Fig. 4b), We want to extract the products concerned about (C10 and C12 narrow fraction) from the top or bottom of the DWC to ensure the quality of the extraction in industrial production. The C8–C9, C10–C12, and C13–C29 products were extracted from the DWC Col-21, respectively. Subsequently, The C10–C12 products were pumped into DWC Col-22, and then the C10, C11, and C12 products were extracted from the DWC Col-22, respectively. Meanwhile, the C13–C29 products were pumped into DWC Col-23, and the C13, C14–C18, and C19–C29 products were extracted from the DWC Col-23, respectively. We adopted IDWC because it is convenient to control the product quality of the C10 and C12 narrow fractions.

For the DDWC separation sequence (Fig. 4c), the C8–C9, C10, and C11–C29 products were extracted from the DWC Col-31, respectively. The C11–C29 products were pumped into DWC Col-32, and then the C11, C12, and C13–C29 products were extracted from the DWC Col-32, respectively. Meanwhile, the C13–C29 systems were pumped into DWC Col-23, and the C13, C14–C18, and C19–C29 products were extracted from the DWC Col-23, respectively. The process which is similar to the traditional distillation process was adopted because it can be modified directly based on the conventional distillation separation.

The reboiler duty optimization results of the total theoretical trays (N_T/N_{TM}), feed stage (F_S), condenser duty (Q_C), and reboiler duty (Q_R) of the three separation processes are shown in Table 1. It can be seen that compared with the TDS process, the reboiler load of the IDWC process and the DDWC process were reduced by 4.7% (i.e., 804 kW) and 15.4% (i.e., 2612 kW) respectively and the condenser duty of the IDWC process and the DDWC process were reduced by 7.7% (i.e., 1302 kW) and 19.3% (i.e., 3260 kW), respectively. The reboiler load of the DDWC process is reduced by 11.2% (i.e., 1808 kW) than that of the IDWC process which the energy consumption difference is mainly reflected in the first module of the separation sequence. The production flow rate in the middle section of the DDWC process is much smaller than that of the IDWC process so that the load in the tower is lower, so the reboiler duty is also lower. Therefore, the DWC process can significantly reduce energy consumption in multi-component separation which will have a great application in the separation of F–T oil.

3.2 C10 and C12 α-olefins separation process simulation

The C10 and C12 normal olefins and alkanes' separation feed were the F–T heavy oil initial separation products with oxygenated component removed. The raw materials for the separation process of C10 and C12 normal olefins and alkanes are shown in Table S7.

The separation processes of C10 and C12 normal olefins and alkanes are shown in Figs. 5 and 6, respectively. The products are 1-decene and 1-dodecene, respectively, with a purity of 95.0 wt%. For the separation process of these two products, a design specification was set that the reflux ratio changes to ensure the product quality from the top. As mentioned earlier, the pressure of two towers of the DPTD process was adjusted so that the temperature of the condenser in the rectifying section is higher than the temperature of the reboiler in the stripping section by more than 10 °C.

The C10 and C12 normal olefins and alkanes' TD are shown in Figs. 5a and 6a, respectively.

In Fig. 5b, the DPTD rectifying section is Col-42 operating at 3.5 kPa, while the stripping section is Col-43 operating at 18 kPa. The reboiler of Col-42 and the condenser of Col-43 are thermally coupled through the main heat exchanger. Since the condenser duty of the DPTD process is greater than that of the reboiler duty, Col-43 requires an auxiliary condenser. Mass transfer is carried out between Col-42 and Col-43 through a throttle valve and a compressor. In Fig. 6b, The C12 normal olefins and alkanes' DPTD process is similar to C10.

The reboiler duty optimization results of the total theoretical stage number (N_T), feed stage (F_S), condenser duty (Q_C), and reboiler duty (Q_R) of TD are shown in Table S8. If the distillation column is changed to the DPTD process, this means that the reboiler duty and condenser duty of 12988 kW and 3512 kW will be saved in C10 and C12 processes, respectively. And a certain amount of heat exchanger cost can be saved. However, DPTD requires an additional compressor and requires electrical energy to drive the compressor to operate compared with TD. Therefore, it is necessary to find a balance between the electrical energy consumed and the thermal energy saved. Anyway, the DPTD process can be applied to the α-olefin separation process to reduce the capital cost in the α-olefin separation process.

4 Economic estimation

In this part, the total annual cost (TAC) of the two procedures of F–T heavy oil separation is estimated, and the optimal parameters of the tower equipment are obtained with

Table 1 Summary of optimal reboiler duty of three F–T synthetic oil separation processes

Column	N_T/N_{TM}	F_S	RR	Q_R (kW)	Q_C (kW)
TDS process					
Col-11	21	13	6.89	1604	− 2880
Col-12	29	14	3.37	3107	− 2363
Col-13	30	15	3.45	3087	− 2707
Col-14	37	18	3.55	3227	− 2793
Col-15	30	16	3.77	2721	− 2726
Col-16	19	7	0.36	3252	− 3401
IDWC process					
Col-21	34	16	11.97	5034	− 4746
Col-22	39	19	9.70	5902	− 5766
Col-23	28	8	8.40	5258	− 5056
DDWC process					
Col-31	29	16	11.00	3960	− 4452
Col-32	45	19	5.60	5168	− 4102
Col-33	28	8	8.40	5258	− 5056

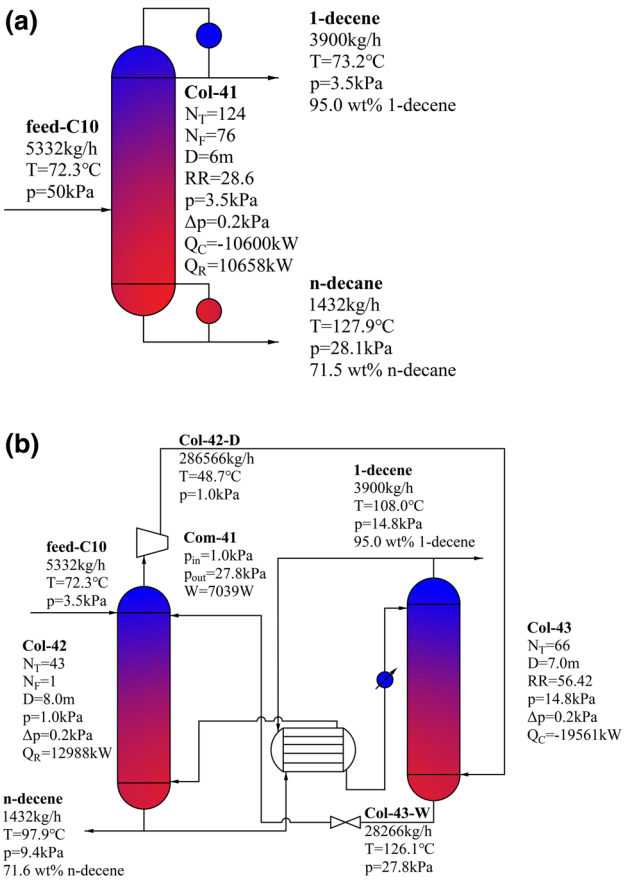

Fig. 5 Process and simulation results of the C10 α-olefins separation. **a** TD process, **b** DPTD process

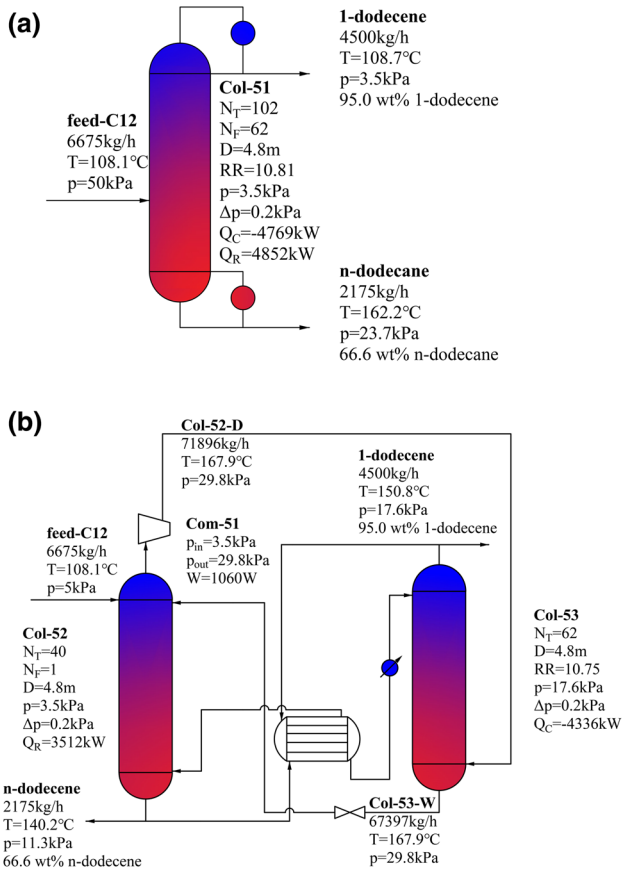

Fig. 6 Process and simulation results of the C12 α-olefins separation. **a** TD process, **b** DPTD process

TAC as the optimization goal as shown in Figs. 4, 5 and 6. Meanwhile, we made a TAC comparison of the different separation processes in the two procedures and found a low-cost method to separate linear α-olefins from F–T heavy oil.

TAC can be obtained by Eq. (8), which mainly includes capital cost and operational cost. Capital cost includes tower, heat exchanger, packing, and compressor cost, while the operational cost mainly includes electricity, heating steam, and condensing water cost. Other cost is too little to be considered. The payback period was usually 3 years in the industry.

$$\mathrm{TAC} = \text{operational cost} + \frac{\text{capital cost}}{\text{payback period}} \tag{8}$$

The capital cost of the column includes the cost of the column body and the cost of packing. The tower body cost in the capital cost was calculated by Eq. (9) where h and d represent the height of the tower and the diameter of the tower obtained from Aspen, respectively. The traditional distillation column β takes 1 while DWC takes 1.1 (Green and Southard 2019). For DWC, the tower diameter is replaced by the diameter of the traditional distillation tower under the

same parameters. The packing is Mellapak which HETP is 0.3 m (Fitz et al. 1999), and the cost of packing are calculated by multiplying the price of the packing by the volume of the tower. The price of the filler (Douglas 1988) is shown in Table S10 in Supplementary Material.

$$\mathrm{Cost}_{\mathrm{column}} = 28047\,\beta\left(\frac{d}{m}\right)^{1.066}\left(\frac{h}{m}\right)^{0.802} \tag{9}$$

The cost of the heat exchanger is obtained from Eq. (10). The heat exchanger area A is calculated by the heat transfer formula. The total heat transfer coefficients of the reboiler and condenser are 500 W/(K m^2) and 910 W/(K m^2) respectively, and the total heat-transfer coefficient of the heat exchanger is 700 W/(K m^2). The cost of the compressor (Calise et al. 2007) was obtained from Eq. (11), where W represented the work consumed.

$$\mathrm{Cost}_{\text{heat exchanger}} = 5563.07\left(\frac{A}{m^2}\right)^{0.65} \tag{10}$$

$$\mathrm{Cost}_{\text{compressor}} = 91562\left(\frac{\mathrm{W}}{445}\right)^{0.67} \tag{11}$$

The operational cost was calculated based on the heat load of heat exchangers and the power of the compressor. For the compressor, the isentropic efficiency is 0.75 and the mechanical efficiency is 0.95. The prices of utility are shown in Table S10. The cost of steam, cooling water, and electricity (Al-Arfaj and Luyben 2002; Douglas 1988; Green and Southard 2019) is as follows Eqs. (12)–(14). Details of the capital cost for those processes are also shown in Table S11 in Supplementary Material.

$$\mathrm{Cost}_{\text{steam}} = 63504C_s\frac{Q_{\mathrm{R}}}{\lambda_{\mathrm{V}}} \tag{12}$$

$$\mathrm{Cost}_{\text{cooling water}} = 689C_{\mathrm{W}}Q_{\mathrm{C}} \tag{13}$$

$$\mathrm{Cost}_{\text{electricity}} = C_{\mathrm{E}}W_{\mathrm{com}} \times 8000 \times 3600 \tag{14}$$

4.1 F–T heavy oil separation process simulation

The optimization logic targeting TAC is shown in Fig. 4b. The TAC optimization results of the total stage number (N_T/N_{TM}), reboiler load (Q_R), and condenser load (Q_C) for the three separation configurations are summarized in Tables S9 and S12 in Supplementary Material. The economic estimation results of the three F–T heavy oil separation processes are shown in Table 2. Since DWC couples two traditional columns into one column, a reboiler and condenser can be saved, so the DWC process can reduce the capital price. As expected, the capital cost of the IDWC and the DDWC processes is reduced by 13.0% (i.e., 3.5×10^5\$) and 17.1% (i.e., 4.6×10^5\$) compared to the TDS process, respectively. The TAC, operating cost, and capital cost of the initial separation process of three F–T heavy oil are shown in Fig. 7a.

The duty of the reboiler and condenser of DWC is lower than that of TDS, which reduces the consumption of the steam and condensate. Therefore, the operational cost of IDWC process and DDWC process is reduced by 3.7% (i.e., 3.5×10^5\$) and 13.0% (i.e., 1.23×10^6 \$) compared with TDS process. However, the DWC process increases the consumption of high-pressure steam compared with TDS, which undoubtedly reduces the possibility of DWC achieving lower TAC. In addition, operational costs account for 77%–80% in three processes, thus the DWC process which reduces the back mix that improves thermal efficiency can significantly reduce TAC. Therefore, the TAC of the DDWC process is 13.8% (i.e., 1.68×10^6 \$) and 8.5% (i.e., 9.7×10^5 \$) lower than the TDS process and the IDWC process, respectively. Besides the lower reboiler load of the DDWC process, the DDWC process can also use low-pressure steam as a heat source is also a general reason. It can be seen that DDWC is the most economical separation process for separating F–T heavy oil.

4.2 C10 and C12 *α*-olefins separation process simulation

The TAC optimization results of the total stage number (N_T/N_{TM}), reboiler load (Q_R), condenser load (Q_C), and compressor power (Q_{comp}) for the two separations are shown in Table S13 in Supplementary Material. Meanwhile, Table 3 summarizes the cost results of the C10 and C12 normal olefins and alkanes' separation processes. For the C12 normal olefins and alkanes' DPTD process, the Col-43 condenser can transfer heat to the Col-42 reboiler, but the Col-42 condenser duty is larger, so only a small amount of condensed water is required. Therefore, a lot of energy consumption can be saved in the DPTD process. Nevertheless, the cost of the compressor and the corresponding electricity cost also account for a larger proportion of the DPTD process. The TAC, operating cost, and capital cost of the normal olefins and alkanes' separation process are shown in Fig. 7b. In general, the TAC reduces by about 47.5% (i.e., 1.88×10^6\$) for

Table 2 Summary of TAC of three F–T heavy oil separation processes

Item	TPC	IDWC	DDWC
TAC	1214	1143	1046
Operating cost	945	910	822
Capital cost	269	234	223

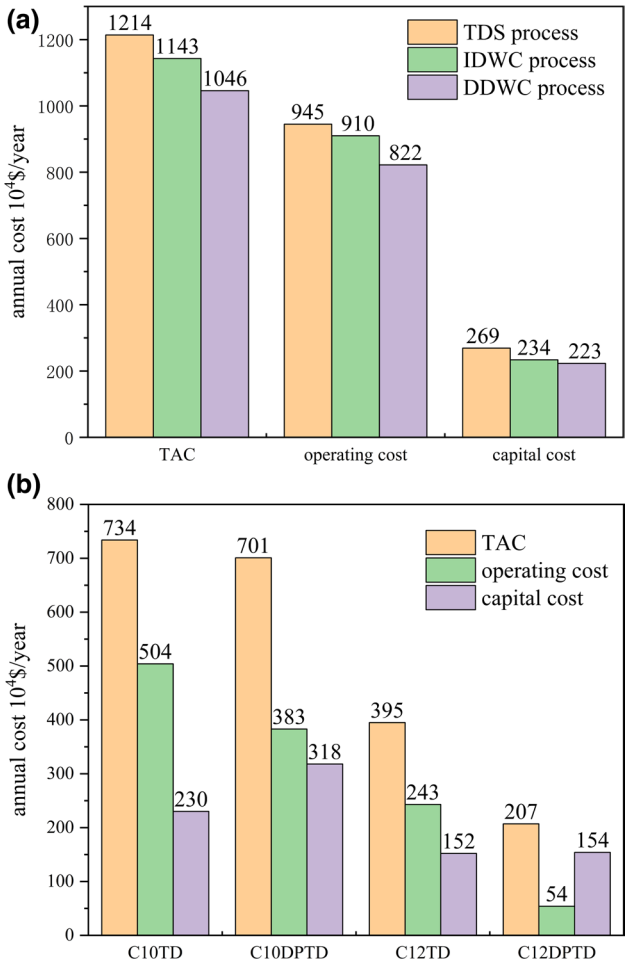

Fig. 7 TAC of two separation procedures for F–T heavy oil. **a** TAC of F–T oil separation process, **b** TAC of narrow fraction separation process

Table 3 Summary of TAC of normal olefins and alkanes' separation processes

Item	C10TD	C10DPTD	C12TD	C12DPTD
TAC	734	701	535	340
Operating cost	504	383	340	137
Capital cost	230	318	196	203

the DPTD processes. Therefore, the DPTD process can be used for the separation of 1-dodecene. However, limited by thermodynamics, the separation of 1-decene and *n*-decane in the high-pressure column required a large reflux ratio and the number of trays for the C10 normal olefins and alkanes' DPTD process. It caused the circulation flow rate and the compression ratio of the compressor to be too large, which makes the compressor and electricity cost account for a relatively large amount, but the DPTD process still saves cost 4.5% (i.e., 3.3×10^5 \$) than the TD process. Therefore, the DPTD technology is a better choice during the normal olefins and alkanes' separation process.

5 Conclusions

The vapor–liquid equilibrium (VLE) data measurement of 1-dodecene & *n*-dodecane is verified by the Gibbs–Duhem equation, which shows that the data obtained is effective and can be imported into the Aspen Plus. Therefore, the simulation accuracy of the normal olefins and alkanes' separation process can be improved. Then, the three processes of F–T heavy oil and two processes of normal olefins and alkanes were simulated and optimized by Aspen Plus V11. The results show that, compared with TDS, the IDWC and DDWC processes can reduce energy consumption by about 4.7% (i.e., 804 kW) and 15.4% (i.e., 2612 kW), respectively, while TAC by about 5.8% (i.e., 7.1×10^5 \$) and 13.8% (i.e., 1.68×10^6 \$), respectively. In addition, under the same product purity and distillation rate, the TAC of the DPTD process is lower than the corresponding TD by 4.5% (i.e., 3.3×10^5 \$) and 47.5% (i.e., 1.88×10^6 \$), respectively. Therefore, the combination of the DDWC process and the DPTD process can separate linear α-olefins from F–T oil at a low cost. This represents two novel technologies and will also have broad prospects in other multi-component separation and purification.

Supplementary Information The online version contains supplementary material available at https://doi.org/10.1007/s40789-022-00527-8.

Acknowledgements The authors are grateful for the financial support from the Key Research and Development Program of Ningxia (Nos. 2018BDE02057, 2019NDYFLX0001), and the Haihe Laboratory of Sustainable Chemical Transformations. The authors also thank the reviewers for their insightful comments and suggestions.

Declarations

competing interest The authors declare no conflict of interest.

References

Al-Arfaj MA, Luyben WL (2002) Control study of ethyl tert-butyl ether reactive distillation. Ind Eng Chem Res 41(16):3784–3796. https://doi.org/10.1021/ie010432y

Belov G, Matkovsky P (2010) Processes for the production of higher linear α-olefins. Pet Chem 50(4):296–302. https://doi.org/10.1134/S0965544110040055

Calise F, d'Accadia MD, Vanoli L, von Spakovsky MR (2007) Full load synthesis/design optimization of a hybrid SOFC–GT power plant. Energy 32(4):446–458. https://doi.org/10.1016/j.energy.2006.06.016

Choi GN (1997) Design and economics of a Fischer–Tropsch plant for converting natural gas to liquid transportation fuels. Fuel Energy Abstr 4(38):222

da Cunha S, Rangaiah G, Hidajat K (2018) Design, optimization, and retrofit of the formic acid process I: base case design and dividing-wall column retrofit. Ind Eng Chem Res 57(29):9554–9570. https://doi.org/10.1021/acs.iecr.8b00883

De Klerk A (2012) Fischer–Tropsch refining. Wiley, South Africa

Dejanović I, Matijašević L, Olujić Ž (2010) Dividing wall column—a breakthrough towards sustainable distilling. Chem Eng Process 49(6):559–580. https://doi.org/10.1016/j.cep.2010.04.001

Dixon JT, Green MJ, Hess FM, Morgan DH (2004) Advances in selective ethylene trimerisation—a critical overview. J Organomet Chem 689(23):3641–3668. https://doi.org/10.1016/j.jorganchem.2004.06.008

Douglas JM (1988) Conceptual design of chemical processes. McGraw-Hill education, New York

Dry M, Steynberg A (2004) Studies in surface science and catalysis. Elsevier, Amsterdam

Egaña A, Sanz O, Merino D, Moriones X, Montes M (2018) Fischer–Tropsch synthesis intensification in foam structures. Ind Eng Chem Res 57(31):10187–10197. https://doi.org/10.1021/acs.iecr.8b01492

Fischer F, Tropsch H (1923) The preparation of synthetic oil mixtures (synthol) from carbon monoxide and hydrogen. Brennst Chem 4:276–285

Fitz CW, Kunesh JG, Shariat A (1999) Performance of structured packing in a commercial-scale column at pressures of 0.02–27.6 bar. Ind Eng Chem Res 38(2):512–518. https://doi.org/10.1021/ie9709300

Fredenslund A (2012) Vapor–liquid equilibria using UNIFAC: a group-contribution method. Elsevier, Amsterdam

Ge XH (2014). The study of the separation of n-hydrocarbons from high temperature oil products of Fischer–Tropsch synthesis: Tianjin University

Gao X, Zhao Y, Yuan W, Liu S, Li X, Li H, Wang S, Lu X (2019) Thermodynamic fundamentals and energy efficiency for the separation and highly valued utilization of light naphtha from Fischer–Tropsch synthesis. Ind Eng Chem Res 58(21):9118–9126. https://doi.org/10.1021/acs.iecr.9b01002

Green DW, Southard MZ (2019) Perry's chemical engineers' handbook. McGraw-Hill Education, New York

Greiner E, Gubler R, Inoguchi Y (2004) Linear alpha olefins. Chemical economics handbook marketing research report. Stanford Research Institute, Menlo Park

Herington E (1951) Test for consistency of experimental isobaric vapor–liquid equilibrium data. J Inst Pet 39:357–361

Kaibel G (1987) Distillation-columns with longitudinal subdivision. Chem Ing Tec 59(6):533–533

Kang JW, Diky V, Chirico RD, Magee JW, Muzny CD, Abdulagatov I, Kazakov AF, Frenkel M (2010) Quality assessment algorithm for vapor–liquid equilibrium data. J Chem Eng Data 55(9):3631–3640. https://doi.org/10.1021/je1002169

Leckel D (2009) Diesel production from Fischer–Tropsch: the past, the present, and new concepts. Energy Fuels 23(5):2342–2358. https://doi.org/10.1021/ef900064c

Li H, Han M, Gao X, Li X (2014) Isobaric vapor–liquid equilibrium for binary system of cinnamaldehyde+ benzaldehyde at 10, 20 and 30 kPa. Fluid Phase Equilib 364:62–66. https://doi.org/10.1016/j.fluid.2013.12.002

Li H, Huang W, Li X, Gao X (2016) Application of the aldolization reaction in separating the mixture of ethylene glycol and 1, 2-butanediol: thermodynamics and new separation process. Ind Eng Chem Res 55(37):9994–10003. https://doi.org/10.1021/acs.iecr.6b02469

Li H, Li X, Luo M (2008) Different pressure thermally coupled distillation technology for energy saving. Chem Ind Eng Progress 27(7):1125–1128

Li H, Zhao Z, Qin J, Wang R, Li X, Gao X (2018) Reversible reaction-assisted intensification process for separating the azeotropic mixture of ethanediol and 1, 2-butanediol: vapor–liquid equilibrium and economic evaluation. Ind Eng Chem Res 57(14):5083–5092. https://doi.org/10.1021/acs.iecr.7b04921

Liu X, Zhang Y, Li M, Li X, Li G, Wang Y, Gao J (2018) Isobaric vapor–liquid equilibrium for three binary systems of ethyl acetate+ propyl acetate, ethyl acetate+ propylene carbonate, and propyl acetate+ propylene carbonate at 101.3 kPa. J Chem Eng Data 63(5):1588–1595. https://doi.org/10.1021/acs.jced.7b01107

Muleja AA, Yao Y, Glasser D, Hildebrandt D (2017) Variation of the short-chain paraffin and olefin formation rates with time for a cobalt Fischer–Tropsch catalyst. Ind Eng Chem Res 56(2):469–478. https://doi.org/10.1021/acs.iecr.6b03512

Mi Q (2017). Studies on the separation of long-chain olefin/paraffin from F–T synthetic oil mixture: North University of China.

Nakhaei Pour A, Housaindokht MR, Kamali Shahri SM (2018) Fischer–Tropsch synthesis over cobalt/CNTs catalysts: functionalized support and catalyst preparation effect on activity and kinetic parameters. Ind Eng Chem Res 57(41):13639–13649. https://doi.org/10.1021/acs.iecr.8b02485

Petlyuk FB (1965) Thermodynamicly optimal method for separating multicomponent mixtures. Int Chem Eng 5:555–561

Schultz MA, Stewart DG, Harris JM, Rosenblum SP, Shakur MS (2002) Reduce costs with dividing-wall columns. Chem Eng Prog 98(5):64–71

Valderrama JO, Faúndez CA, Campusano R (2019) An overview of a thermodynamic consistency test of phase equilibrium data. Application of the versatile VPT equation of state to check data of mixtures containing a gas solute and an ionic liquid solvent. J Chem Thermodyn 131:122–132. https://doi.org/10.1016/j.jct.2018.09.019

Wang MM (2016) The study of the separation of n-alkanes and α-alkenes from oil product of Fischer–Tropsch synthesis: Hebei University of Technology

Wang MM, Zhang MQ, Gao ZL, Liu S (2016) Vapor-liquid equilibrium of C10 and dimethyl phthalate in vacuum. Chem Eng (China) 44(10):32–36

Yamamoto M, Narahara H (2004) The measurement of vapor-Liquid equilibrium data by headspace gas chromatography. Sumitomo Kagaku I:1–10

Yildirim Ö, Kiss AA, Kenig EY (2011) Dividing wall columns in chemical process industry: a review on current activities. Sep Purif Technol 80(3):403–417. https://doi.org/10.1016/j.seppur.2011.05.009

Zhang L, Liu J, Li X, Li H, Jiang B, Xiao X (2015) Separations of different binary hydrocarbon mixtures using pressure swing thermally coupled distillation process. Sep Purif Technol 50(1):148–157. https://doi.org/10.1080/01496395.2014.948000